JOURNAL OF GEOPHYSICAL RESEARCH, VOL. 102, NO. D22, PAGES 26,263–26,281, NOVEMBER 27, 1997

Radar observations of gravity waves over Jicamarca, Peru during the CADRE campaign

Dennis M. Riggin[1] and David C. Fritts[1]
Colorado Research Associates/NWRA, Boulder

Clinton D. Fawcett and Erhan Kudeki
Department of Electrical and Computer Engineering, University of Illinois, Urbana

Matthew H. Hitchman
Department of Atmospheric and Oceanic Sciences, University of Wisconsin-Madison

Abstract. We present results obtained with the mesosphere-stratosphere-troposphere (MST) radar at Jicamarca, Peru, from three 10-day experiments in January 1993, March 1994, and August 1994. Horizontal and vertical velocities were measured over ranges spanning the lower part of the stratosphere and most of the mesosphere. In the stratosphere, the fluctuating part of the wind field was found to be dominated by inertia-gravity waves. Sinusoids of different period were fit to the velocity time series using a least squares procedure. The dominant periods of the inertia-gravity wave motions were found to be 1.5 days for the January 1993 experiment and 2.1 days for the August 1994 experiment. For the January 1993 experiment, the amplitudes and phases of the inertia-gravity wave oscillations were extracted for the vertical as well as the horizontal components. The vertical amplitude of the 1.5-day period wave was small ($<0.1\,\mathrm{m\,s^{-1}}$), but measurable with the Jicamarca radar. The intrinsic periods of the inertia-gravity waves were inferred from the fits using two different methods. The first method predicted the intrinsic period using the orbital ellipses traced out in time by fits to the horizontal winds. The second method used information taken from the vertical as well as the horizontal fits. The values of intrinsic period made using the second method were found to have much less scatter than the values inferred solely from the orbital ellipses. The momentum flux estimates in both the stratosphere and mesosphere were found to depend significantly on the exact methodology used. A technique was adopted whereby estimates were formed only when radial velocities were measured simultaneously on both beams of a coplanar beam pair. Most of the total wave stress was usually contributed by waves at periods ≥ 4 hours in the stratosphere and ≥ 1 hour in the mesosphere. In the stratosphere, localized layers of enhanced momentum flux were sometimes observed. The obvious anticorrelation between the shear of the mean wind and the momentum flux in these layers suggests that they were caused by in situ generation of waves by the Kelvin-Helmholtz instability, rather than gravity waves propagating from lower levels. At short periods, momentum flux spectra in the stratosphere and mesosphere showed numerous positive and negative peaks. A correlation analysis revealed that the high-frequency peaks were associated with discrete wave packets. The short-scale waves associated with these packets were fairly isotropic in their direction of propagation, and due to cancellation they contributed little net momentum.

1. Introduction

In an earlier paper [*Riggin et al.*, 1995] (hereinafter referred to as P1), we discussed radar observations of inertia-gravity wave (IGW) motions in the lower stratosphere during late January 1993. The January 1993 experiment was the first of three Coupling and Dynamics of Regions Equatorial (CADRE) 10-day experiments

[1]Also at Program in Atmospheric and Oceanic Sciences, University of Colorado, Boulder

Paper number 96JD03675.
0148-0227/97/96JD-03675$09.00

performed at Jicamarca. This paper presents a more quantitative analysis of the IGW motions observed during the first CADRE experiment at Jicamarca, and also greatly expands on P1. Our results now span most of the mesosphere, as well as the lower stratosphere. Seasonal comparisons are made possible by the inclusion of results from the two more recent 10-day experiments.

The importance of the vertical flux of horizontal momentum in interactions between waves and the mean winds is now well established in the literature [e.g., *Fritts,* 1984]. However, little is known about the relative contribution of different frequencies of gravity waves to the total flux, and in fact the frequency dependence of the flux has not been measured at all in the tropical middle atmosphere. There is mounting evidence from observations that the motion field in the tropical, lower stratosphere is typically dominated by inertia-gravity waves with periods of 1–3 days [e.g., *Cadet and Teitelbaum,* 1979; *Maekawa et al.,* 1984; *Cornish and Larsen,* 1990; *Maruyama,* 1994; *Sato et al.,* 1994; *Tsuda et al.,* 1994; *Eckermann et al.,* 1995; *Cho,* 1995; P1; *Karoly et al.,* 1996; *Palo and Avery,* 1996; *Shimizu and Tsuda,* this issue; *Sato and Dunkerton,* this issue]. Although the presence of these large-amplitude motions suggests a significant contribution of low frequencies to the total momentum flux, *Eckermann and Hocking* [1989] have argued that many of these cases of seemingly low-frequency, quasi-monochromatic waves were actually random superpositions of much higher frequency waves. The determination of wave intrinsic properties and the spectral dependence of the flux were among the principal goals of the CADRE experiments at Jicamarca, and our results will be used to address this question.

In section 2 we describe the mode of operation of the Jicamarca radar and explain the data analysis procedures. Section 3 summarizes the background conditions in the stratosphere and mesosphere during the three experiments. Estimates of the propagation parameters associated with inertia-gravity wave events are presented in section 4. In section 5, measurements of momentum flux are presented with subsections on the results in the stratosphere and mesosphere. The paper concludes with a discussion of the main results in section 6.

2. Data Collection and Analysis

The Jicamarca VHF (50 MHz) radar near Lima, Peru (12°S, 77°W) was operated for 10-day measurement campaigns during January 20–29, 1993, March 10–19, 1994, and August 16–25, 1994. Usable data were limited to 19.2–32.0 km in the stratosphere for the first two experiments. This lower height limit was imposed by (1) the use of relatively long complementary-coded pulses (20-baud with a 2.67 μs or 400 m baud length), and (2) the need to avoid ground clutter and provide adequate time for receiver recovery. For the last experiment, a technique for decoding the truncated ranges [*Spano et al.,* 1991] was implemented that allowed usable velocity estimates to be obtained down to 9.2 km. In the mesosphere, usable data were obtained from 60 to 90 km for all three experiments. Measurements were obtained only during the daylight hours (~10 hours each day), because mesospheric backscatter depends on the presence of free electrons produced by photoionization. The stratospheric signal-to-noise (S/N) ratio does not degrade during the nighttime hours, but the radar was shut down during these periods. No data were obtained from the intermediate heights of 32–60 km, because the index of refraction variations responsible for backscatter in the stratosphere and the ionization layers responsible for backscatter in the mesosphere are mostly absent from this region. The maximum altitude of the mesospheric data was limited by the lower edge of the equatorial electrojet. The electrojet usually has a much larger scattering cross section than mesospheric ionization above 95 km and masks mesospheric echoes. Although several of the plots shown later extend up to 90 km, the results above 85 km should be regarded with caution. Electrojet contamination tends to cause an underestimate in the magnitude of the wind at these uppermost ranges.

The antenna array was divided into four quadrants, phased to provide beams in the north, south, east, and west directions at zenith angles of 2.5°. The small zenith angle is necessary to avoid sidelobes but is probably nearly ideal for measuring vertical velocities. Bias due to specular reflection from horizontal layers are avoided because the half-width, two-way, half-power beam widths in the beam tilt direction are only ~0.6°. Details on the processing used to obtain line-of-sight velocities from the raw data are given by *Hitchman et al.* [this issue]. The time resolution of the line-of-sight velocity estimates was 2 min in the stratosphere and 1 min in the mesosphere, considerably shorter than the respective buoyancy periods (~4 min at 30 km and ~5 min at 80 km). Thus, the sampling rate was sufficient to resolve waves at the highest intrinsic frequencies unless they were strongly Dopper-shifted. The data were thresholded on the basis of S/N, spectral width, and other criteria. Additional outlier removal was performed by comparing the radial velocity on the east beam with the negative of the radial velocity observed simultaneously on the west beam. If the eastward radial beam velocity at a particular range gate differed from the negative of the westward radial velocity by more than 1.75 $m\,s^{-1}$ in the stratosphere, or by more than 5.25 $m\,s^{-1}$ in the mesosphere, it was rejected. When projected onto the eastward horizontal direction, these radial velocity differences correspond to horizontal velocity differences of 40 $m\,s^{-1}$ in the stratosphere and 120 $m\,s^{-1}$ in the mesosphere and are almost certainly not physical. The same procedure was performed on the north/south coplanar beam pair. Northward, eastward, and vertical velocities were derived from the radial components following the procedure described by

Hitchman et al. [1992]. For samples where good velocity estimates were obtained on the conjugate beam pair (e.g., north/south as well as east/west), all four beams were used in forming an estimate of the vertical velocity (w). Adding the information from the conjugate beam pair (when available) reduced the scatter in w profiles, although the improvement was relatively minor. However, note that only the coplanar beams were used to form the w estimates used in momentum flux calculations. Using all four beams for this purpose can introduce contamination from the horizontal flux of horizontal momentum. Additional averaging of the velocities was performed to estimate the motions associated with longer timescales. When averaging the data, further outlier removal was performed by detrending the data in each bin (i.e., subtracting a linear trend) and applying Chauvenet's criterion which is more tolerant of outliers as the number of points in the distribution increases [*Young,* 1962]. Two-hour averages offset by 1 hour were used to study IGWs and other low-frequency structures and campaign (10-day) averages were used to study the mean structure.

Vertical fluxes of horizontal momentum are usually estimated in the time domain using the method of *Vincent and Reid* [1983],

$$P = \frac{\langle [v_e - \langle v_e \rangle] \rangle^2 - \langle [v_w - \langle v_w \rangle] \rangle^2}{2\sin(2\theta)}. \quad (1)$$

Here, P is the zonal momentum flux, the angle brackets denote averaging in time, and $v_{e,w}$ are the east/west radial velocities. An analogous equation can be written for the meridional momentum flux. For the case of simultaneous measurements on a coplanar (e.g, east/west) beam pair, the radial velocities can be projected into the horizontal and vertical directions. P can then be equivalently written in terms of the horizontal and vertical velocities as

$$P = \langle u' w' \rangle, \quad (2)$$

where the primes denote the fluctuating part of the velocity. Note that (1) (unlike (2)) makes no assumption of simultaneity of measurements on the coplanar beam pair. When we compared vertical profiles of momentum flux, we found that imposing a requirement of simultaneity yielded a result with much less scatter. Possible reasons for the difference are (1) without a simultaneous signal on both beams we were precluded from using one of the criteria for outlier rejection described previously, (2) the treatment of the velocities as random variables assumes that the averaging is performed over times much longer than characteristic periods of the waves contributing to the flux (not the case as we show later), and (3) the near verticality of the beams magnifies errors by causing (1) to be a ratio of very small numbers.

Momentum flux spectra are calculated from the cospectra of the horizontal and vertical velocities. In the zonal direction these take the form

$$p(\omega) = 2\,\mathrm{Re}[U(\omega)W^*(\omega)], \quad (3)$$

where U, W are the FFT's of u', w' (the primes denote fluctuating part), the factor of 2 comes from taking only positive frequencies, the asterisk denotes complex conjugate, and Re denote the real part. Note that (3) is the frequency domain counterpart of (2) and that (1) also has a counterpart in the frequency domain that has been applied to calculate momentum flux spectra [*Nakamura et al.,* 1993]. Momentum flux spectra will be presented in energy-content form, (i.e., $\omega p(\omega)$), so that momentum flux values at different frequencies can be compared directly. Note that the momentum flux spectra can be used to estimate the total momentum flux over a time interval since

$$P = \sum_i p(\omega_i). \quad (4)$$

Since (3) involves a complex product of FFT's, it can only be applied over altitudes with a minimal number of data gaps. However, we did employ (4) as a means of testing our algorithms and found the values of P calculated in the frequency domain were nearly identical to those calculated in the time domain. In the stratosphere we calculated momentum flux spectra only up to a height of 25 km. At this uppermost height, no more than 10% of the velocity estimates were found to be missing after preprocessing, and these data gaps were linearly interpolated. Momentum flux spectra were also calculated in the mesosphere, with some averaging of the velocities in height (as explained later) to reduce the number of data gaps.

If the frequency of a particular dominant wave packet is known during a time interval, the momentum flux due to this component can be determined using a singular value decomposition (SVD), least squares fitting procedure. In section 5.1 we show some results obtained using this technique. A sinusoidal fit to u' can be written in the form $U\cos(\omega_i t - \phi_u)$ and similarly for w', where ω_i is the frequency selected for the fit. The momentum flux corresponding to the selected frequency is calculated from the fits by

$$p(\omega_i) = \frac{U\,W}{2}\cos(\phi_u - \phi_w). \quad (5)$$

The fitting window is slid forward in time to give $p(\omega_i)$ as a function of time. In practice we found that a window of four wave cycles length was a reasonable compromise between time and frequency localization. With this choice of a window length, the half power band edges are at $\omega_i \pm 0.11\omega_i$. Further details on the SVD technique are given in P1.

3. Mean Structure

The mean structure of the near-equatorial motion field over Jicamarca during the three measurement campaigns is displayed in Figure 1 with campaign (10-

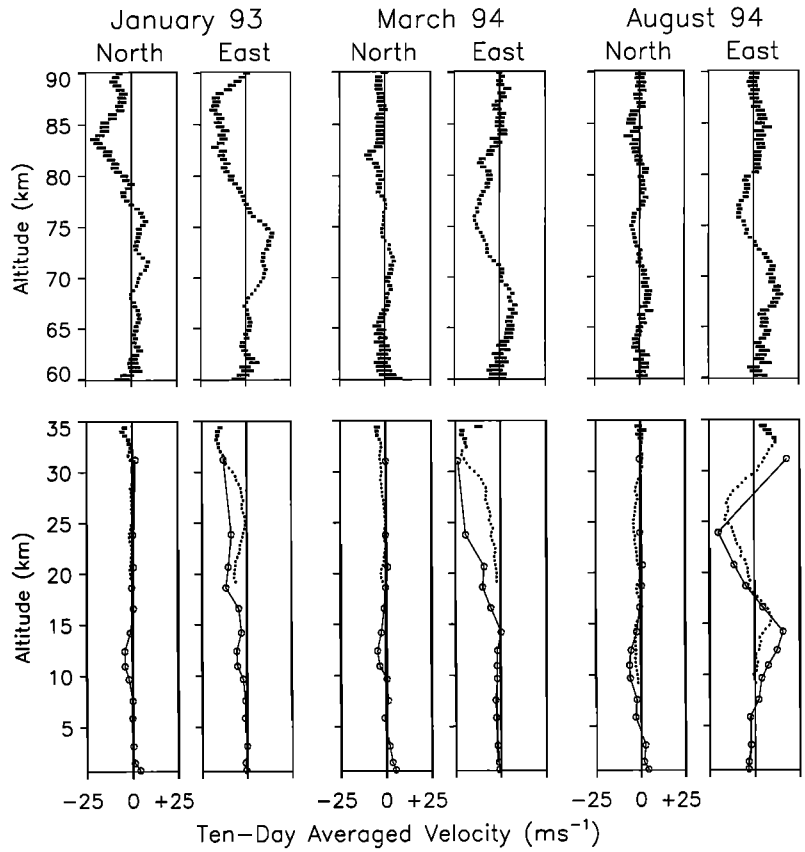

Figure 1. Campaign averages of the radar winds in the stratosphere and mesosphere during the three Jicamarca experiments (error bars as symbols) and averages of ECMWF winds for the coordinates of Jicamarca (open dots).

day) averages of the horizontal velocity components in the stratosphere and mesosphere. The error bars at each range gate show the uncertainty in the winds as $\pm 2\sigma/\sqrt{n}$, where n is the number of wind estimates during the 10 days and σ is the standard deviation of the estimates. In addition to showing the winds measured by the radar, the bottom panels show winds derived from 10-day averages of European Centre for Medium-Range Weather Forecasts (ECMWF) analyses as open dots. The ECMWF analyses [*Trenberth and Olson*, 1988] have 2.5° resolution and the winds plotted were taken from the grid point closest to Jicamarca. The radar and ECMWF winds agree fairly well over the altitudes at which they overlap, which gives us confidence in (at least) the sign and approximate magnitude of the winds in the troposphere over Jicamarca. Calculations made with the ECMWF temperatures indicate that the tropopause was at ~16–17 km during all three campaigns.

For the January 1993 period the zonal wind profile in the stratosphere exhibits a curvature (bowed toward the east) that is characteristic of the quasi-biennial oscillation (QBO) in its eastward phase. Although the QBO was eastward, the zonal wind over Jicamarca was westward due to influences described by *Hitchman et al.* [this issue]. At the uppermost heights (~35 km) sampled by the radar in the stratosphere, the QBO was just beginning its transition to westward (K. Labitzke, unpublished data, 1994). By March 1994 the QBO was in its westward phase as reflected in the zonal velocities. Five months later during August 1994, it was well into its transition back into the eastward phase.

The zonal wind field in the mesosphere during the three Jicamarca experiments was characterized by positive and negative lobes separated by about ~10 km showing the dominance of the mesopause semiannual oscillation (MSAO) in the zonal wind. This vertical structure is similar to that previously measured by rocketsonde [Hirota, 1978] over Ascension Island (8°S), although the rocket-derived winds were considerably larger in magnitude. During the January 1993 experiment the meridional mean wind measured by the radar was as large as the zonal wind showing the influence of motions other than the MSAO. However, as an artifact of sampling the winds only during the daylight hours, waves with periods near 1 day can show up spuriously in the campaign mean. At the latitude of Jicamarca the mesospheric diurnal tide reportedly had an amplitude of ~10–20 m s^{-1} during January 1993 and a somewhat smaller zonal amplitude [*Deng et al.*, 1997]. Wind variations of roughly this magnitude were observed over Jicamarca during January 1993 as shown Figure 1 and

the ~10 km vertical separation of the positive and negative peaks is consistent with the ~20 km wavelength of the diurnal tide [*Lieberman and Hays,* 1994]. Thus, the mean winds during January 1993 were probably a superposition of the mesopause semiannual oscillation (MSAO) with effects due to the uneven sampling of the diurnal tide. The radar measured only weak meridional winds during the March and August 1994 experiments, suggesting minimal tidal influence in these cases. In addition to the larger-scale (15 km) structure, the meridional wind in the mesosphere during January 1993 exhibited smaller-scale (~5 km) structure that could be a signature of local inertial instability. Structure due to IGWs is probably removed by the 10-day averaging. The March 1994 and August 1994 zonal mesospheric wind profiles are similar, as one would expect given the MSAO's 6-month period. *Hitchman et al.* [this issue] fully discuss the climatology in the tropical stratosphere and mesosphere during the three Jicamarca campaigns.

4. Inertia-Gravity Wave Observations

Inertia-gravity waves (IGWs) are gravity waves with intrinsic periods that are on the order of (but less than) the inertial period. At the latitude of Jicamarca, the inertial period ($2\pi/|f|$, where f is the local Coriolis parameter) is ~58 hours. Prior observations of IGWs were reviewed in P1 so, aside from some recently published results, we confine our introductory discussion to some equations that are useful for IGW parameter estimation. In the limits $k \ll m$ and $m^2 \gg 1/4H^2$, where k represents the horizontal (not necessarily zonal) wavenumber in the direction of propagation, m is the vertical wavenumber, and H is the atmospheric mass density scale height, the dispersion relation for low-frequency gravity waves can be written in the simplified form,

$$\omega^2 = N^2 \frac{k^2}{m^2} + f^2 . \tag{6}$$

We will later also make use of polarization relations which relate the amplitudes and phases of the three orthogonal components of wave velocity. If we assume variations of the form $e^{i(-\omega t + kr + mz)}$, where r is along the direction of wave propagation in the horizontal plane, these relations can be written in the form

$$\frac{v'_{\parallel}}{v'_{\perp}} = i\frac{\omega}{f} \tag{7}$$

$$\frac{v'_{\parallel}}{w'} = -\frac{m}{k} . \tag{8}$$

Here, the primes denote the fluctuating components of the velocity, $v'_{\parallel}$ is the horizontal perturbation along the direction of wave propagation, and $v'_{\perp}$ is the horizontal velocity perturbation perpendicular to the direction of wave propagation. The perpendicular direction is defined as toward the left when looking along the direction of wave propagation, and m is negative for the usual (downward) sense of vertical phase propagation. It is easily shown from (7) that the wind vector associated with an IGW follows an orbital motion that is traced out in the anticyclonic direction as either time or height increases. Cyclonic rotation will be observed (in both space and time) when the phase is upward propagating and can also be observed (in time) when $-\mathbf{k}\cdot\mathbf{u} > \omega$, where ω is the intrinsic frequency of the wave.

One of the challenges of radar analysis of IGWs is determining the intrinsic frequency (ω) which is related to the observed frequency (ω_0) by $\omega = \omega_0 - \mathbf{k}\cdot\bar{\mathbf{u}}$. *Hirota and Niki* [1985] were among the first to determine ω experimentally, using (7) and the orbital ellipses traced out by the winds in height. Recently, a cross-spectral technique has been used [*Cho,* 1995] for a more objective determination of ω from either the height or time dependence of the orbital motions. Long-period waves observed in the lower stratosphere over Arecibo had previously been attributed to relatively high frequency mountain waves, Doppler shifted by the winds to a low ω_0 [*Hines,* 1989], but the cross-spectral results demonstrated that the waves were actually IGWs. *Eckermann* [1996] has recently demonstrated the need for a refinement to the technique, although this does not appear to invalidate the Arecibo results. The diurnal data gaps at Jicamarca prevent the easy application of the cross-spectral technique, but the availability of vertical velocities at Jicamarca provides an alternate means of calculating ω using (8) instead of (7).

Figures 2 and 3 show horizontal velocity contours for the January 1993 and August 1994 experiments. The

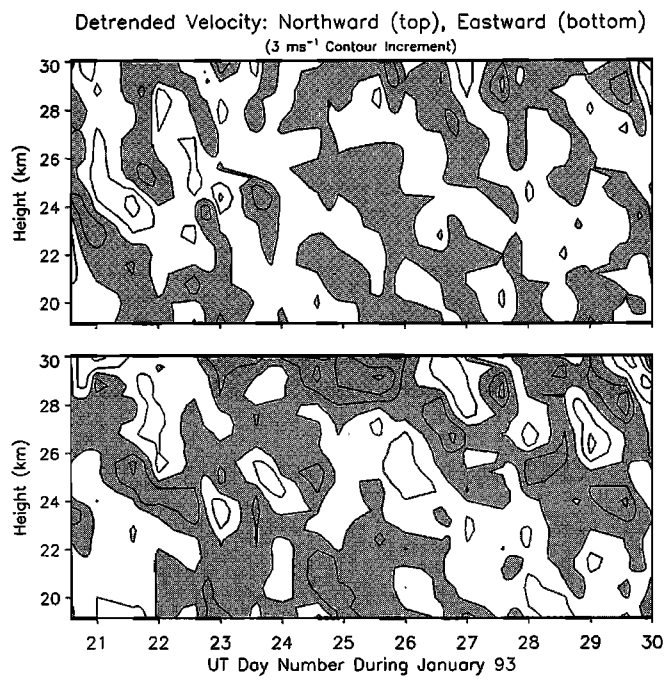

Figure 2. Contours of (top) northward velocity and (bottom) eastward velocity in the stratosphere with increments of 3 m s^{-1}. Southward and westward velocities are shaded.

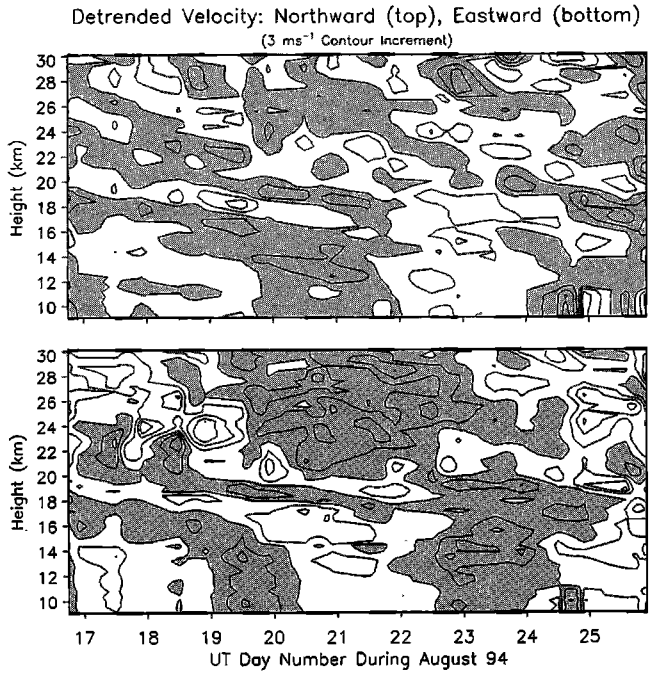

Figure 3. Same as Figure 2, but for the August 1994 campaign.

wave motions have been emphasized by detrending the velocity time series at each height over the 10 days. The contours are interpolated across data gaps during the local nighttime hours (denoted by a relatively thinner line for the x axis). Both plots show evidence of IGW activity in the temporal modulation of the horizontal wind field on timescales longer than 1 day. The March 1994 velocity contours (not shown) also indicated the presence of IGW activity, although it was weaker and less coherent than during the other experiments. It should be remembered that waves with periods near 1 day are suppressed due to the diurnal gaps, so we cannot be certain that the contours reveal the dominant IGW motions. The waves have a slow downward phase velocity as seen by the gradual downward progression of points of constant phase (e.g., the dividing line between shaded and unshaded regions). During the January 1993 campaign, the wind shear descended at ~3 km/day, while during August 1994 the rate of descent was ~1.5 km/day. Combining these vertical phase velocities with the vertical wavelengths (~5 km during January 1993 and ~3 km during August 1994) yields IGW periods of ~1.7 days and ~2.0 days for the two campaign periods, respectively. These periods and vertical wavelengths are very similar to those reported from radiosonde balloon observations in the tropical stratosphere [e.g., *Shimizu and Tsuda,* this issue].

These features have usually been attributed to IGWs. However, *Eckermann and Hocking* [1989] argued that observations in the tropics purporting to show long-period IGWs do not reflect the normal climatology. They claimed that many, if not most, of these apparently long-period waves are actually superpositions of much shorter period waves. Although we are unable to fully address the climatology question, the well-defined downward phase progression over several days during the January 1993 and August 1994 experiments leads us to believe that we were not observing a beat product of higher-frequency waves. We will later present additional evidence that the waves were of low intrinsic period.

A more quantitative analysis was performed on the January 1993 data by applying least squares sinusoidal fits to the detrended time series of u', v', and w' at each height. Different wave periods were applied to the data and then compared to select the period yielding the largest amplitude. The 1.5-day period yielded the best fit for the January 1993 period, and a 2.1-day period yielded the best fit for the August 1994 experiment. These values are close to the rough estimates of the periods inferred from the downward trends in the wind contours. Figure 4 presents the amplitudes and phases obtained from fits applied to 4-day segments (overlapped by 2 days) and fits applied to 10-day campaign segments. Similar fits were performed in P1, but only to the horizontal components of velocity. Over some heights, the phase of the fits to u', v', and w' have a similar dependence with height, and the inferred vertical wavelength over these regions is ~5.3 km. The zonal amplitudes are ~2–5 m s^{-1}; the meridional amplitudes are somewhat smaller (implying a direction of propagation that is more zonal than meridional), and the vertical amplitudes are 1–3 cm s^{-1}. Two different techniques can be applied to determine the intrinsic period of the wave from the fits to the velocity components. We will refer to these techniques in the following discussion as methods I and II.

Method I derives the intrinsic period from the orbital ellipses traced out by the tip of the horizontal velocity vector as a function of time. Thus, it is similar to hodograph analysis which uses the orbits traced out as a function of height. The fits to u' and v' shown in Figure 4 provide the information needed to apply method I. It is relatively simple to solve numerically for $v'_{\parallel}$ and $v'_{\perp}$ from u' and v' at each height. The ratios $v'_{\parallel}/v'_{\perp}$ were then substituted into (7) to find ω. Figure 5 shows the intrinsic frequencies inferred using method I, depicted as open dots/dotted lines. The first four panels are values derived from fits to overlapping 4-day data segments and the last panel from fits to the full 10 days. The frequency is normalized by f, with logarithmic horizontal axes ranging over 1–100 so the vertical grid line through the center of each plot corresponds to one tenth of an inertial period or 5.8 hours. Estimates of ω/f for which $v'_{\parallel} < 1$ m s^{-1} are not plotted, because relatively poor fits were obtained in cases of extremely small wave amplitude. There is considerable scatter in the results, although they are not inconsistent with the 18-hour intrinsic period estimated from a hodograph analysis in P1.

Method II makes use of the vertical as well as the horizontal velocity amplitude of the wave and involves a few more steps. The first step is to obtain the veloc-

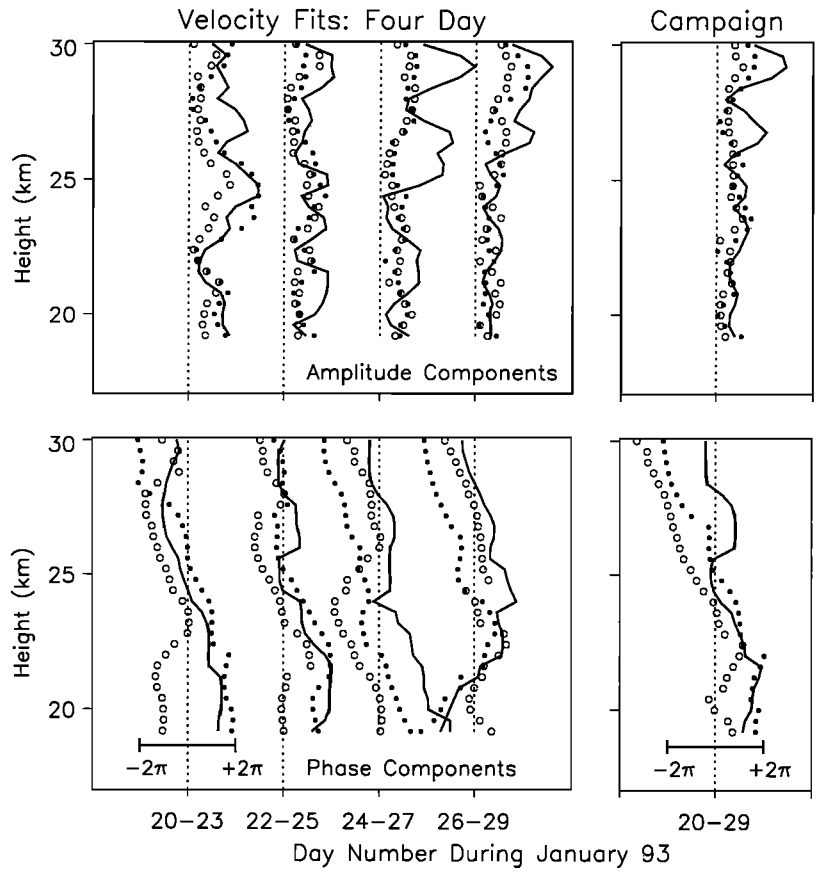

Figure 4. Fit of a 1.5-day period sinusoid to (left) overlapping 4-day segments and to (right) entire 10-day campaign showing (line) zonal phase/amplitude fit, (solid dots) meridional fit, and (open dots) zonal fit. The vertical grid lines in the amplitude fits (upper two panels) are offset by $5\,\mathrm{m\,s^{-1}}$ for the horizontal wind fits and by $0.1\,\mathrm{m\,s^{-1}}$ for the vertical fit.

ity amplitudes corresponding to the major axis of the orbital ellipses ($v'_{\|}$), although this was already found when applying method I. The amplitude ratios of w' to $v'_{\|}$ are computed at each height and then (8) and (6) (assuming N=0.023 $\mathrm{s^{-1}}$) are applied to determine the intrinsic period. The values calculated using method II (shown as solid dots/solid lines in Figure 5) are much less erratic than those calculated from method I. Where the wave had the largest amplitude and we have greatest confidence in the fits (e.g., fits for January 26–29 above 26 km), method II yields ω/f~6–10, which corresponds to intrinsic wave periods of ~6–10 hours. The horizontal wavelength estimated using method II is also proportionately smaller, 400–700 km, as compared with ~2000 km predicted from method I or the hodograph analysis in P1. The IGW during the January 1993

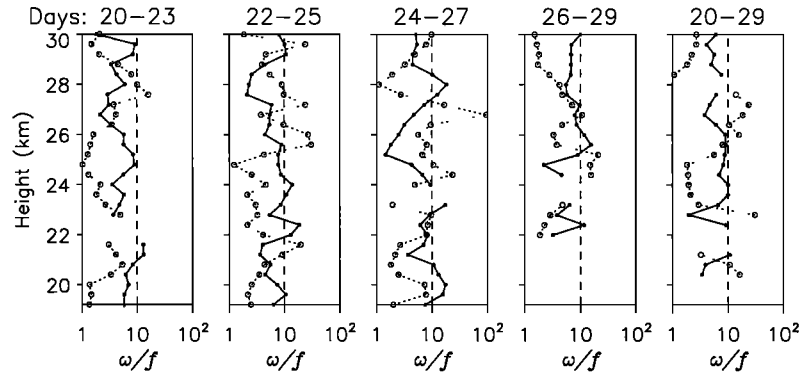

Figure 5. Intrinsic frequency normalized by Coriolis parameter for the January 1993 campaign calculated using method I (open dots) and using method II (solid dots). The first four panels show results derived from fits to 4-day segments and the panel furthest to the right was derived from a fit to the full ten days.

campaign was Doppler downshifted to a much longer observed period by a mean wind that was strongly westward. The sign of the zonal wind and Doppler shift together imply that the wave was eastward propagating. A wavelength of 550 km and an intrinsic period of 8 hours are consistent with a westward velocity of $15\,m\,s^{-1}$. This calculated zonal velocity is in reasonable agreement with the observed velocity during the January 1993 campaign. Of course the combination of longer intrinsic periods and longer wavelengths are also consistent, so it is impossible to distinguish the correct intrinsic period on this basis alone. It would be interesting to discover whether it is generally the case that method II predicts an intrinsic period shorter than method I, but we were unable to repeat this analysis for the other campaigns. The IGW activity shown in Figure 3 was a superposition of low-frequency wave motions which prevented us from obtaining consistent fits of a single-frequency component. Thus, it is not yet clear whether use of the vertical wave amplitudes has wide applicability for determining the propagation characteristics of IGWs.

More can be learned about the dominant gravity waves from the standard deviation (σ) of the wind components. Table 1 shows the σ values computed over 5 km height ranges for u', v', and w'. The values in parentheses are standard deviations calculated from 2-hour binned data while those not in parentheses were calculated from the data at 2-min time resolution. The coarse binning reduces the standard deviations in the horizontal plane to ~70% of their value computed from the 2-min data while the vertical standard deviations are ~25% as large. In the horizontal plane, the motions were highly anisotropic during all three campaigns. Except at the lowest ranges (10–15 km), $\sigma_u/\sigma_v \gtrsim 2$. A slightly larger ratio is obtained from the standard deviations computed from the 2-hour binned velocities. The anisotropies imply that gravity wave propagation in the tropical stratosphere is mostly aligned along the east/west axis regardless of season as previously reported by *Hamilton* [1991].

The standard deviations derived from the 2-hour binned data for the January 1993 experiment are somewhat larger than the estimated IGW amplitudes (see Figure 4), but are well within an order of magnitude, suggesting that the IGW contributed much of the variance. During the August 1994 campaign the horizontal standard deviations were larger and the vertical values smaller. These conditions are probably related to an IGW of a longer period during August 1994, as previously discussed in connection with Figure 3. The ratio σ_u/σ_w is another useful parameter that can be used to characterize the dominant scale size of the motions. As computed from the 2-hour averaged velocities, σ_u/σ_w~80–90 for the January 1993 experiment. Adopting this ratio as a rough estimate of $v_\parallel'/w'$ for the dominant gravity wave, it can be substituted for the left-hand side of (8). Assuming a 5.3 km vertical wavelength (as found from the phase/amplitude fits), (8) yields a horizontal wavelength of 400–500 km, consistent with the method II prediction. The vertical wavelength of the IGW during the August 1994 campaign was ~4 km and σ_u/σ_w was 200–300. Using these values, (8) yields a horizontal wavelength of 800–1,200 km.

5. Momentum Fluxes

Because it is formed from a product of velocities, the momentum flux is an inherently noisy quantity and therefore a relatively long time average must be used to get a reliable estimate of the mean value. For this reason, and because w' is very difficult to measure, the published data on radar derived momentum fluxes are limited. Much of the current understanding of momentum flux relies on theory and numerical models. *Fritts* [1984] used simple theoretical arguments to predict the proportion of momentum flux due to gravity wave motions in the high- and low-frequency parts of the spectrum. A

Table 1. Standard Deviation ($m\,s^{-1}$) of Wind Fluctuations in the Stratosphere

	January 1993			March 1994			August 1994		
Height (km)	σ_u	σ_v	σ_w	σ_u	σ_v	σ_w	σ_u	σ_v	σ_w
10–15	—	—	—	—	—	—	5.1 (3.3)	4.0 (2.8)	0.087 (0.058)
15–20	—	—	—	—	—	—	6.6 (4.5)	3.4 (2.2)	0.078 (0.024)
20–25	5.3 (3.6)	2.8 (1.7)	0.129 (0.045)	5.2 (3.4)	2.7 (1.4)	0.146 (0.044)	10.4 (7.3)	4.2 (2.6)	0.106 (0.025)
25–30	6.1 (3.8)	4.3 (1.9)	0.190 (0.041)	9.8 (6.8)	3.2 (2.1)	0.203 (0.074)	12.9 (9.0)	5.3 (2.8)	0.163 (0.044)

Values in parentheses are derived from 2-hour averaged velocities.

power spectral dependence of the form $E(\omega)\sim\omega^{-\kappa}$ was assumed for the horizontal velocity fluctuations, and the amplitude of the vertical fluctuations was assumed to be related to that of the horizontal fluctuations by $w'/u'\sim\omega/N$. The *Fritts* [1984] result can be written in terms of an intermediate period (T_m), for which the flux integrated over longer periods equals the flux integrated over shorter periods,

$$T_m{}^{\kappa-2} = \frac{1}{2}\left[\left(\frac{N}{2\pi}\right)^{2-\kappa} + \left(\frac{f}{2\pi}\right)^{2-\kappa}\right]. \quad (9)$$

Assuming a κ=5/3 power law as is usually observed in the lower stratosphere [*Fritts et al.*, 1990] and taking appropriate values of parameters for the latitude of Jicamarca (N=0.025s^{-1} and f=3.03×10^{-5}s^{-1}), (9) yields $T_m\approx$25 min. T_m has a very weak dependence on f, and in fact the increase in f with latitude is more than offset by the decrease in N with latitude [e.g., *Yamanaka et al.*, 1996]. The value of T_m is decreased by about ~4 min if we assume

$$\frac{w'}{u'} \sim \frac{\sqrt{\omega^2 - f^2}}{N}, \quad (10)$$

which is consistent with (6) and reflects the fact that vertical IGW propagation and momentum transport ceases as ω approaches f. Thus, the scaling arguments predict that most of the momentum flux is contributed by high frequency waves at all latitudes.

5.1. Stratospheric Momentum Fluxes

Propagating waves, such as mountain waves, gravity waves, Rossby waves and equatorially trapped waves are undoubtedly sources of momentum in the stratosphere. However, there are other contributing processes, such as mesoscale disturbances, frontal motions, and convection. Mountain waves in particular are believed to be sources of significant flux, requiring parameterization in general circulation models of the troposphere and stratosphere [*Palmer et al.*, 1986]. Radar measurements of momentum flux in the stratosphere with the Poker Flat radar [*McAfee et al.*, 1989] and with the MU Radar [*Fukao et al.*, 1988; *Fritts et al.*, 1990] have shown that waves at periods longer than 6 hours contribute most of the total flux. These cases of low-frequency dominance have been attributed to synoptic disturbances or to mountain waves. If mountain waves are the main source, it is surprising that the low-frequency dominance was observed in every experiment, because their observation is dependent on the exact placement of the radar with respect to the terrain, and their excitation is dependent on the wind speed and direction.

Figure 6 shows daily (actually ~10 hour) averaged meridional momentum flux profiles (top) and zonal flux profiles (bottom) from the January 1993 experiment. The flux estimates (shown as solid dots/solid lines) were calculated from data with no prior temporal averaging of the data and thus include the contribution from waves with periods as short as four minutes. Data were

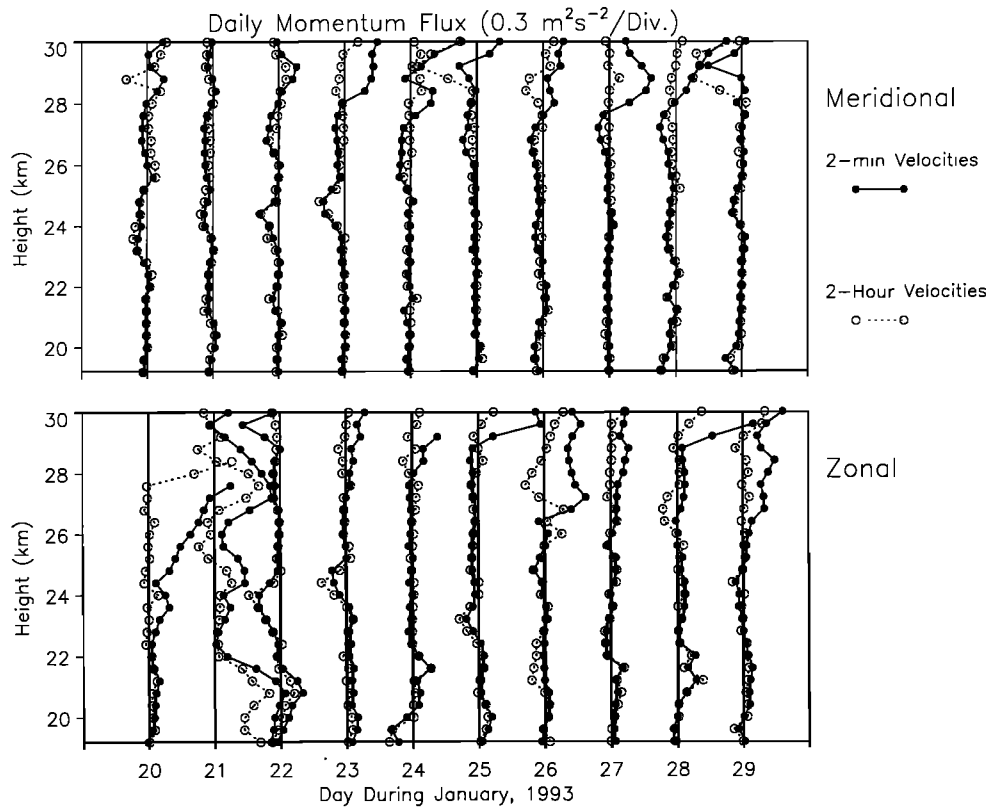

Figure 6. Daily (~10 hour) averaged values of meridional momentum flux (top panel) and zonal momentum flux (bottom panel) in the stratosphere. Profiles are offset by 0.2 m^2 s^{-2}.

included from the adjacent heights when forming the averages to increase the number of velocity products and provide more robust estimates. The profiles, offset by $0.2\,m^2\,s^{-2}$, fluctuate with altitude and do not show a clearly preferred direction. Layers of enhanced momentum flux can be seen in the profiles that appear to persist for more than 1 day. Note in particular the layer at ~25 km in the meridional fluxes during the first four days of the campaign. Daily momentum fluxes for the March 1994 and the August 1994 campaigns are not shown, but were qualitatively similar, i.e., weak and fluctuating in sign with altitude, but with layers of enhanced momentum flux that sometimes persisted for multiple days. To determine the contribution at low frequencies, the data were binned into 2-hour time bins offset by 1 hour and the flux recomputed. The 2-hour averaging corresponds to a Nyquist period of 4 hours. Waves at shorter periods than the Nyquist period (e.g., 3 hours) are attenuated by the averaging, but could still influence the low-frequency momentum flux if they are relatively strong. In spite of the rather drastic averaging that has been applied to the data, the fluxes calculated with the 2-hour velocity averages (plotted as open dots/dashed lines) are almost indistinguishable from the total flux much of the time. However, there are a few time intervals during which the 2-hour momentum fluxes depart significantly from the 2-min values. This is particularly apparent on January 21 and 22 at the upper ranges sampled in the stratosphere. This may be a real effect due to an intermittent source of high-frequency waves, although we cannot pinpoint the cause. The usually observed similarity of the momentum fluxes generated from the 2-hour averaged data to those generated from 2-min data suggests that the net flux is mostly carried by waves with periods $\geq$4 hours.

Having established that the low-frequency component dominates the net momentum flux, a remaining question is whether this component is associated with IGWs or with mountain waves of much shorter intrinsic period that are propagating upstream in the mean flow. The ratio of horizontal to vertical standard deviation was introduced in section 4 to characterize the scale size of the motions. Although the σ_u/σ_w and σ_v/σ_w scale factors have no explicit frequency dependence, the contribution of all but the lowest (extrinsic) frequency waves is suppressed by computing the scale factors from the 2-hour averaged velocities. As derived from 2-hour binned data (see Table 1), $\sigma_u/\sigma_w \approx 80$–$90$ and $\sigma_v/\sigma_w \approx 30$–$40$ for the first two campaigns. Substituting σ_u/σ_w for the left-hand side of (12), with $N=0.023\,s^{-1}$, and $f=3.03\times10^{-5}s^{-1}$, we find intrinsic periods 6–7 hours for the first two campaigns. The same procedure for the August 1994 campaign yields intrinsic periods of ~15–20 hours. This is evidence that the low-frequency momentum flux is due to waves of low intrinsic frequency rather than Doppler shifted mountain waves.

The results plotted in Figure 6 and the estimates of intrinsic period raise the question of whether there is significant momentum flux due to motions with time scales even longer than the 10-hour observing period. To test this supposition, we recomputed the momentum flux over 4-day periods offset by 2 days and for the entire 10-day campaign. For these flux estimates, the mean velocities that are subtracted in (2) are 4-day or campaign averages. Note that the velocities are not evenly sampled over these time segments and, in particular, that the momentum flux contribution from waves with periods near 1 day are either suppressed or may be aliased into the mean due to the diurnal gaps. Figure 7 shows the fluxes obtained, where the vertical grid lines are offset by $0.2\,m^2\,s^{-2}$ and where open dots/dashed lines are the eastward component and solid dots/solid lines are the northward component. The fluxes in Figure 7 were computed from the 2-min time resolution data so they include the total contribution from ultra-low frequencies to high frequencies. A weak low-frequency contribution to the momentum flux shows up over many heights in

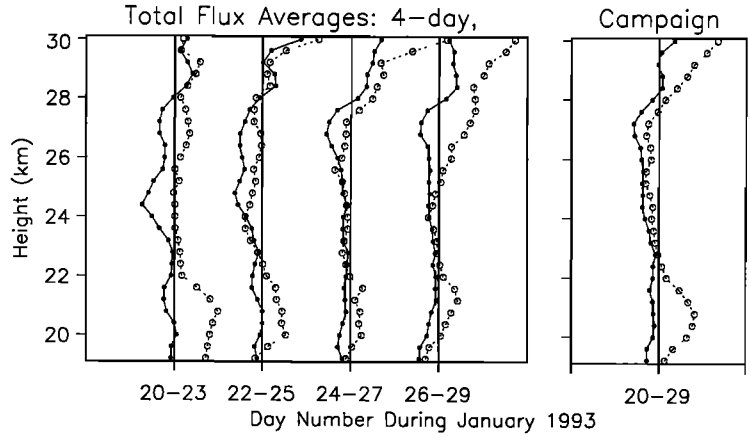

Figure 7. Overlapping 4-day and campaign estimates of zonal momentum flux (open dots) and meridional momentum flux (solid dots) in the stratosphere for the January 1993 campaign. Profiles are offset by $0.2\,m^2\,s^{-2}$.

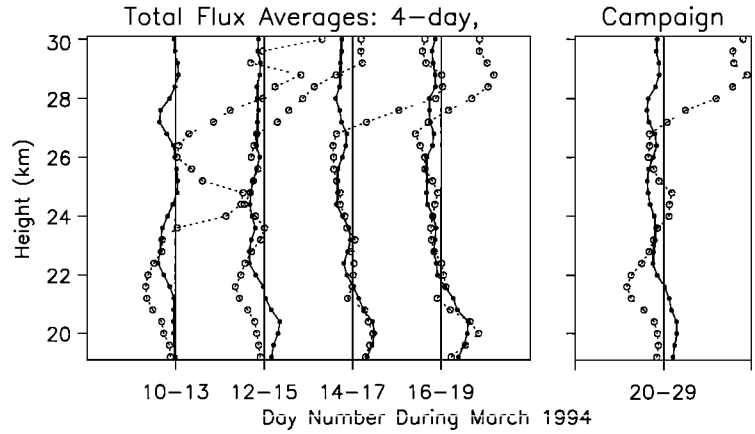

Figure 8. Same as Figure 7, but for the March 1994 campaign.

these 4- and 10-day estimates that does not show up clearly in the daily averaged momentum fluxes. This additional flux is due to waves with periods >10 hours, but we cannot quantify the period due to the nighttime gaps. Because the wave drag is proportional to the vertical convergence of $\rho\langle u'w'\rangle(1-f^2/\omega^2)$ [*Fritts and Vincent,* 1987], the ultra-low-frequency waves are less effective at producing accelerations of the mean flow. The 4-day and campaign averages of momentum fluxes for March 1994 and August 1994 are shown in Figures 8 and 9. Past experiments have demonstrated that the momentum flux is often in the opposite direction of the mean wind, presumably due to selective filtering of the waves by the mean wind [*Fritts and Vincent,* 1987]. A comparison of the zonal wind (Figure 1) and zonal momentum flux (Figure 7) for the January 1993 campaign shows this tendency. The zonal fluxes during March are also anticorrelated with the mean wind, as are the relatively large zonal fluxes above 25 km in the August 1994 results. There is no apparent correlation between the meridional wind and momentum flux, but this is not surprising given the weakness of the mean meridional wind in the stratosphere during all three experiments. The magnitudes of the fluxes we observed in the lower stratosphere were similar during the three experiments and are comparable to those reported from most other radar experiments [e.g., *Fritts et al.,* 1990]. However, they are more than an order of magnitude smaller than the stratospheric fluxes reported from earlier experiments at Jicamarca [*Hitchman et al.,* 1992]. Momentum fluxes derived from radiosonde measurements in the near-equatorial stratosphere [*Sato and Dunkerton,* this issue] are much smaller than our estimates for unknown reasons. The product of 2-hour binned standard deviations $\sigma_u\sigma_w$ is 0.15–0.5 $m^2 s^{-2}$ over the three Jicamarca radar experiments and various height ranges. Although larger than the values of $\langle u'w'\rangle$ displayed in Figures 7, 8, and 9, it is well within the same order of magnitude. This suggests that low-frequency coherent waves produce much of the variance in the stratosphere over Jicamarca.

Turning now to the momentum flux at relatively higher frequencies, we concentrate on the results for January 22, 1993. The momentum fluxes on this day were fairly representative of the results obtained throughout the three experiments. Figure 10 shows 2-hour estimates of the meridional momentum flux (top) and the zonal momentum flux (bottom) overlapped by 1 hour.

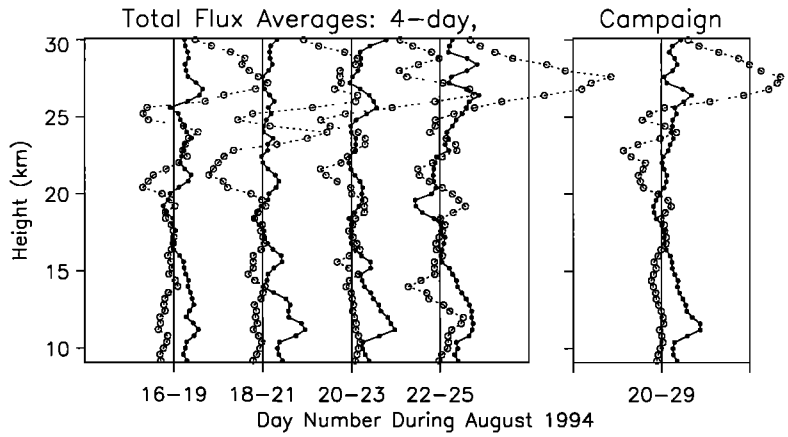

Figure 9. Same as Figures 7 and 8, but for the August 1994 campaign.

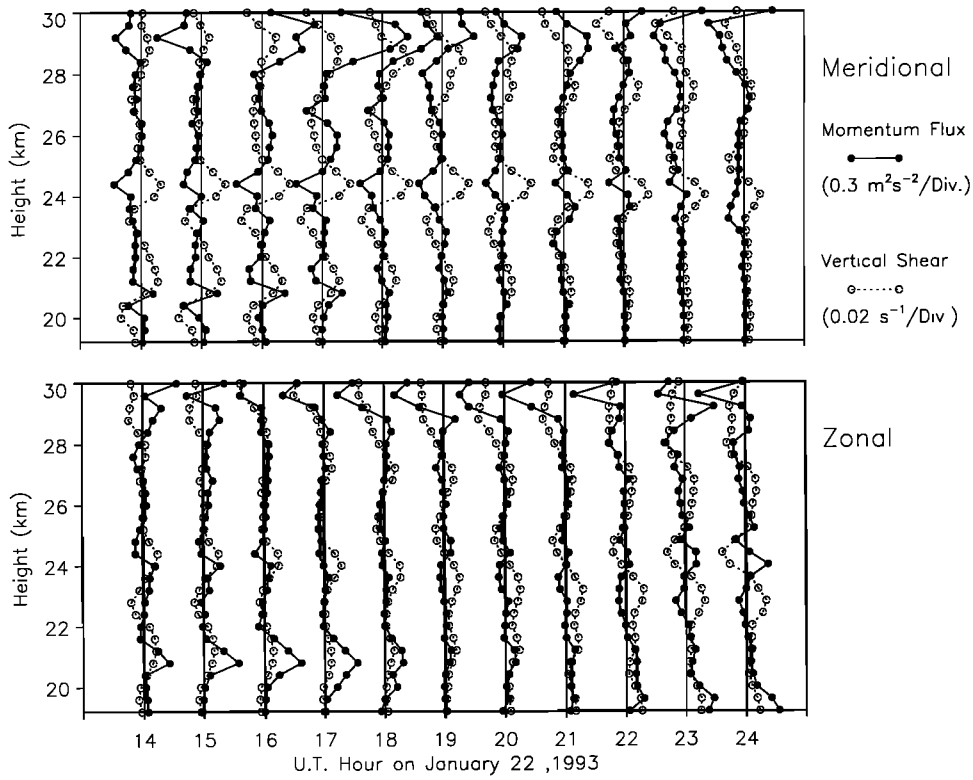

Figure 10. Two-hour momentum flux averages overlapped by 1 hour. Also shown is the shear of the mean wind derived from 2-hour averages of the horizontal winds overlapped by 1 hour.

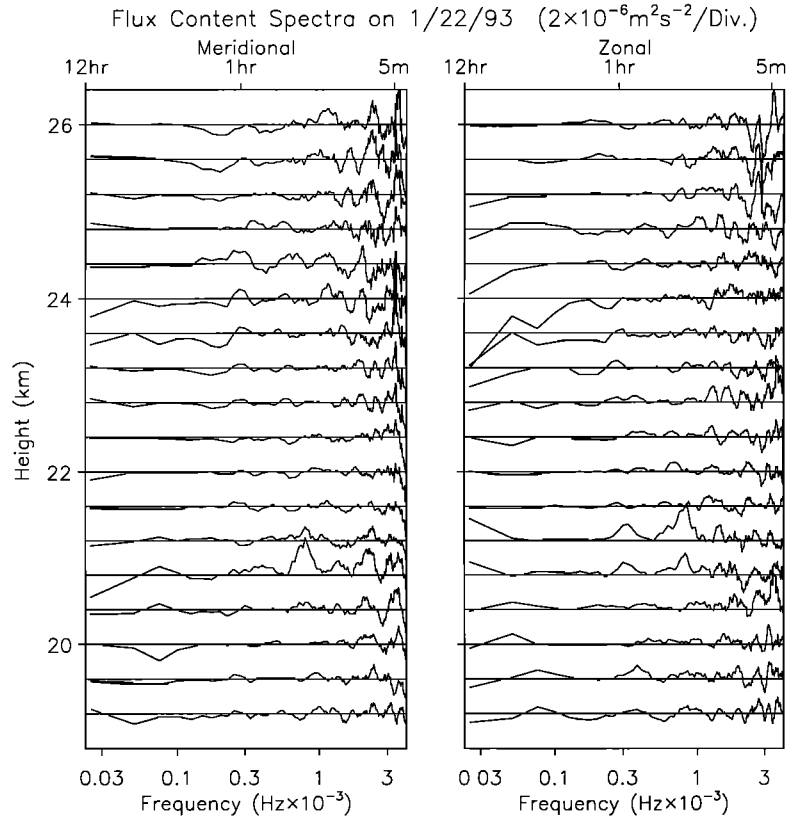

Figure 11. Spectra of (left) meridional momentum flux and (right) zonal momentum flux (right-hand panel) in area preserving form. The spacing between horizontal grid lines is $2\times10^{-6}\mathrm{m}^2\mathrm{s}^{-2}$.

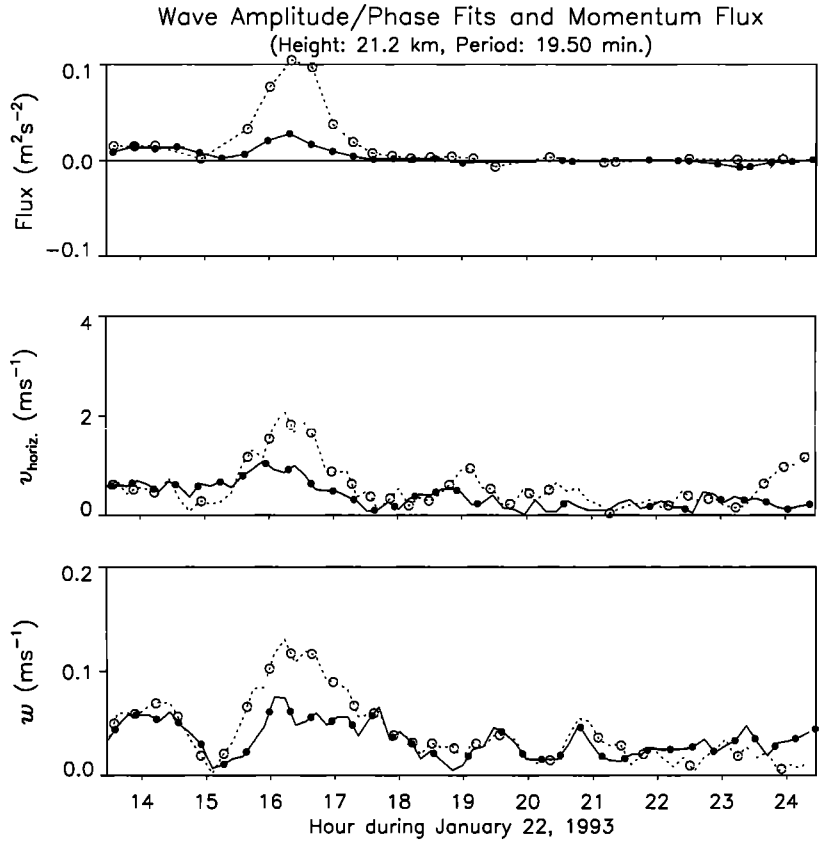

Figure 12. SVD fits performed with four-cycle sliding window at a period of 19.5 min. Phase is portrayed using the dots which correspond to the times of the wave crests. (bottom) Amplitude/phase fit to w' from the east/west beam pair (open dots) and from the north/south beams (solid dots). (middle) Amplitude/phase fit to u' (open dots) and v' (solid dots). (top) Zonal momentum flux (open dots) and meridional momentum flux (solid dots).

The flux is depicted with solid dots/solid lines with profiles offset by $0.2\,m^2s^{-2}$. A conspicuous feature is the ~1-km-thick layers of enhanced momentum flux. In the absence of strong shears, this concentration of momentum flux into narrow layers would not be expected for gravity waves propagating upward through the atmosphere. Thus, we consider dynamical instability as an explanation. The Kelvin-Helmholtz (KH) instability is shear driven, so the fluxes of momentum that arise in response to this instability should be in a direction to oppose (and eventually reduce) the shear. Figure 10 also shows values of shear calculated from 2-hour velocity estimates overlapped by 1 hour and averaged in height using a three-height sliding average. The momentum flux and shear are clearly anticorrelated. The KH instability is thus a plausible explanation for the layers of enhanced flux. A difficulty with this interpretation is that the Richardson number ($Ri=N^2/|\overline{u}_z|^2$) is ~5, well above the usually cited threshold for instability ($Ri=0.25$). The large estimate of Ri does not make the KH instability untenable if one considers that (1) the vertical averaging noted previously caused the shear to be somewhat underestimated, (2) *Hines* [1971] has argued that the $Ri \leq 0.25$ instability criterion is too stringent in some cases, and (3) the presence of large amplitude waves or inertial instability can locally change the stability profile, even to the point of convective instability ($N<0$). The KH instability is difficult to observe because it occurs over small vertical spatial scales, but there is evidence that it is a common process in all regions of the atmosphere [e.g., *Fritts and Rastogi*, 1985; *Nielsen*, 1992].

Figure 11 shows momentum flux spectra from the stratosphere during January 22, 1993, with a separation between the horizontal grid lines of $2\times10^{-6}\,m^2\,s^{-2}$. In this presentation the spectral points are smoothed using a boxcar function with the number of points in the average proportional to the square root of frequency. The spectra were computed from velocity estimates that are independent at each height, but there is obviously a high degree of height-to-height correlation at the lowest frequencies and also for the larger peaks at high frequency. To better understand the behavior of the waves responsible for the peaks in the spectra, we return again to the time domain and calculate the momentum flux for a particular frequency component using the correlation technique described in section 2, i.e., (5). As a test case, we applied the algorithm to the peaks that were identified in the zonal momentum flux at 21.2 km. The peaks in question are the two prominent peaks, at periods of 19.5 min and 53 min in the sixth zonal spectrum from the bottom of Figure 11. Figure 12 (bottom)

presents sliding, four-cycle, amplitude/phase fits to w' for a period of 19.5 min. The phase is represented by the dots that indicate the times of positive extrema in the fitted sinusoid or wave "crests." The open dots/dashed lines are values calculated from the east/west beam pair and the solid dots/solid line are from the north/south beams. Figure 12 (middle) shows the fits to the zonal and meridional wind and two components of momentum flux are shown in the top panel. Note that only coplanar beam information is used when calculating momentum flux for the reasons discussed in section 2. Most of the momentum flux responsible for the peak in the spectrum occurs over a time-span of 1–2 hours. The momentum flux is possibly delivered by the wave packet over an even shorter time-span, because the fitting window is four cycles (~80 min) long. In the case of the 53 min period fit shown in Figure 13, the amplitudes and peak momentum flux are smaller, but they are maintained for a much longer period of time. The peak momentum fluxes associated with particular wave packets in Figures 12 and 13 are comparable in magnitude to the time-integrated momentum fluxes shown in the preceding figures. The picture that emerges from looking at these and other examples is that there are many wave packets with periods less than an hour that individually carry significant momentum. However, they are fairly isotropic in their direction of propagation, and when integrated across the spectrum they contribute only a small net wave stress. The net momentum flux is mainly contributed by waves at periods longer than those associated with the more prominent peaks in the momentum flux spectra. This cancellation of momentum flux contributions has also been demonstrated by applying an innovative analysis technique to radiosonde data [*T. J. Dunkerton,* manuscript in preparation, 1997; *Sato and Dunkerton,* this issue].

5.2. Mesospheric Momentum Fluxes

The main sources of momentum flux in the tropical mesosphere are probably propagating waves, such as gravity waves, planetary waves, and equatorially trapped waves. There is some observational evidence that high-frequency waves cause much of the flux in this region, although perhaps not to the extent that models and theory would suggest. *Fritts and Vincent* [1987] and *Reid and Vincent* [1987] found that 70% of the momentum flux was associated with motions at periods less than 1 hour. *Nakamura et al.* [1993] found that the flux was typically largest at periods of 30 min–1 hour, while *Murphy and Vincent* [1993] reported flux magnitudes that did not depend strongly on wave period. The standard deviations and momentum fluxes in the Jicamarca mesosphere are harder to interpret than those in the stratosphere, because the tides and planetary waves make a significant contribution. For this reason, the standard deviations for the mesosphere are not pre-

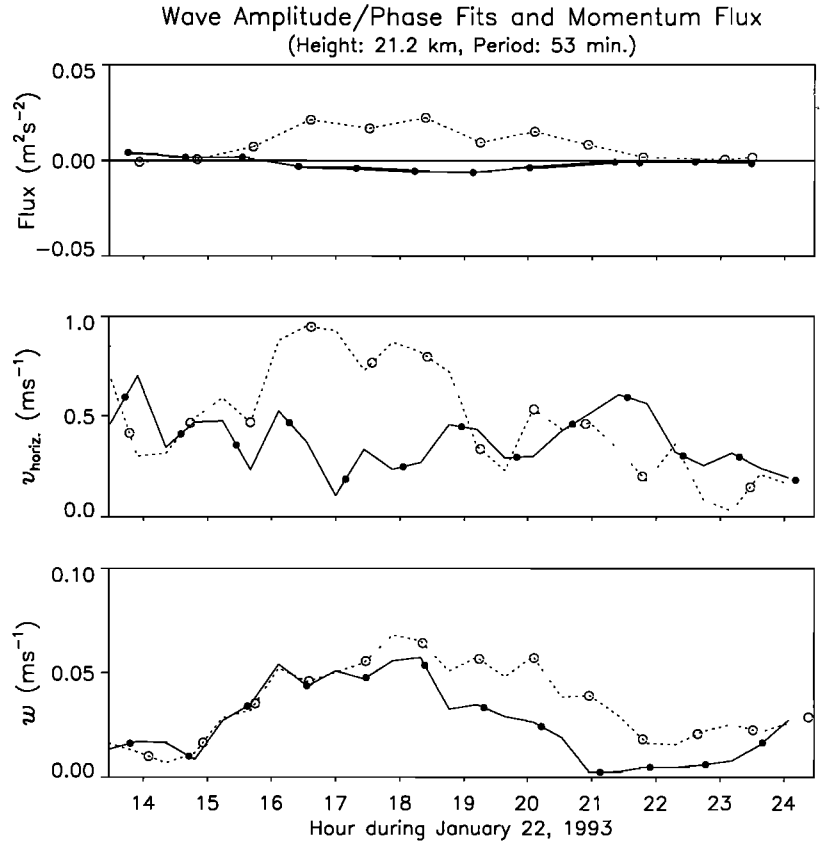

Figure 13. Same as Figure 12, but for period of 53 min.

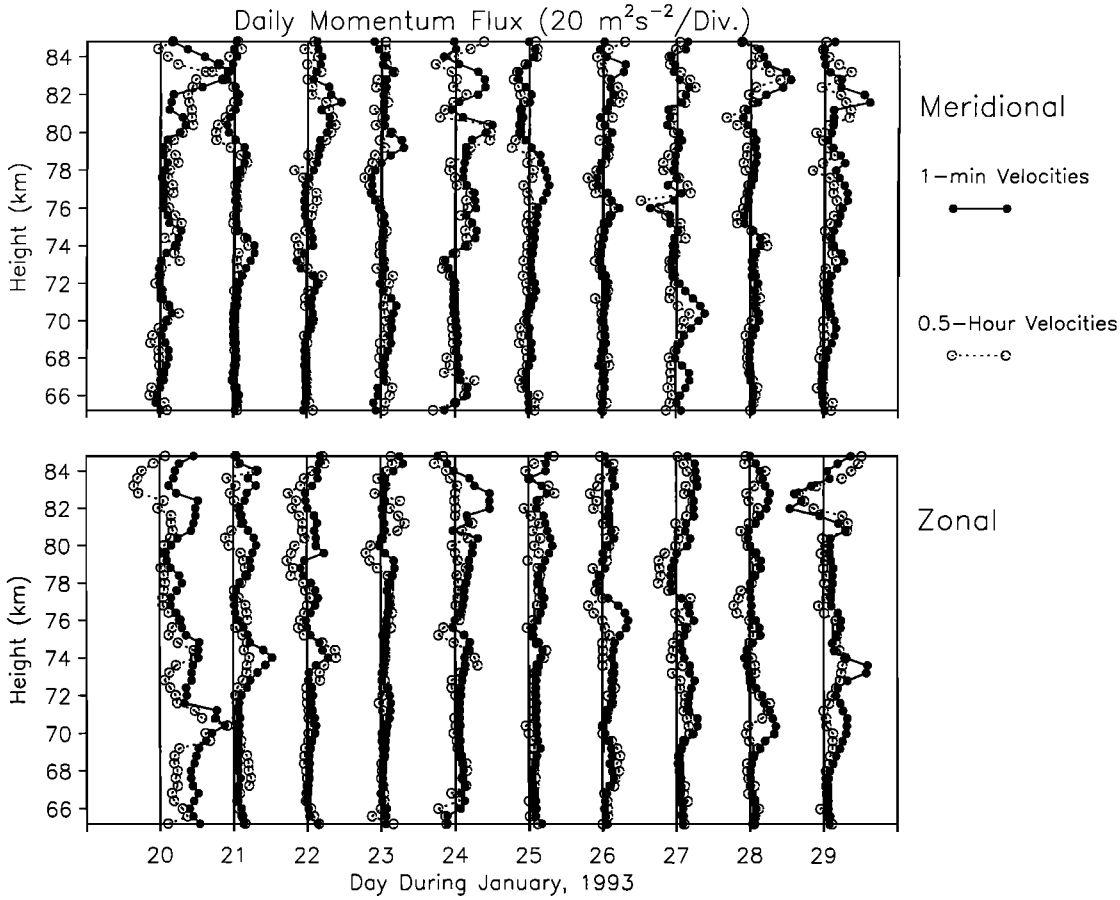

Figure 14. Daily (~12 hour) averaged values of (top) meridional momentum flux and (bottom) zonal momentum flux in the mesosphere. Profiles are offset by $20\,m^2s^{-2}$.

sented. However, it should be mentioned that the standard deviation of the wind in the north-south direction was found to be nearly the same as that in the east-west direction at each height. No evidence was found for a predominantly zonal alignment of the waves as was observed in the stratosphere.

Figure 14 shows daily (~12 hour) averages of momentum flux for the January 1993 campaign as calculated from the 1-min time resolution data (solid dots/solid lines). Both the meridional and zonal fluxes are slightly biased toward the positive direction. The daily momentum fluxes found during an earlier experiment at Jicamarca [*Fritts et al.*, 1992] peaked at $\sim 30\,m^2s^{-2}$, comparable to the $\sim 20\,m^2s^{-2}$ maximum values found during the January 1993 experiment. The fluctuations of momentum flux with altitude shown in Figure 14 are somewhat similar in appearance to the stratospheric profiles of momentum flux shown in Figure 6, but the magnitudes in the mesosphere are ~100 times greater. The momentum fluxes calculated from horizontal and vertical velocities binned into half-hour averages are also shown in Figure 14 (open dots/dashed lines). These binned fluxes approximate the total flux, but fluxes computed from 2-hour, binned data (not shown) were found to deviate considerably from the total flux. Thus, as expected, the momentum fluxes in the mesosphere are less dominated by low-frequency waves than those in the stratosphere. The stratospheric momentum fluxes were usually anticorrelated with the mean wind, while in the mesosphere, this tendency was only seen above ~80 km. Below 80 km we found the mesospheric momentum fluxes were often highly correlated with the mean wind. Figure 15 shows 4-day and 10-day campaign estimates of the momentum flux with profiles offset by $10\,m^2s^{-2}$. These flux estimates are derived from velocities at 1-min resolution. Long-term averages of the fluxes for the other two experiments are not shown, but they were similar in character. *Fritts et al.* [1992 made 6-day estimates of momentum flux at Jicamarca and found peak values of $\sim 30\,m^2s^{-2}$, somewhat larger than the values found during the CADRE experiments. The diurnal tide probably does not directly produce much momentum flux at the altitudes of our observations (<90 km) and the latitude of Jicamarca [*Lieberman and Hays,* 1994]. However, the tide has been reported to cause a very pronounced modulation of the momentum flux due to shorter period gravity waves [*Fritts and Vincent,* 1987]. The unavoidable nighttime gaps in the mesospheric data could cause some bias in the multiday momentum flux estimates, if the fluxes were strongly modulated by the diurnal tide. The mesospheric fluxes could also be affected by the quasi 2-day

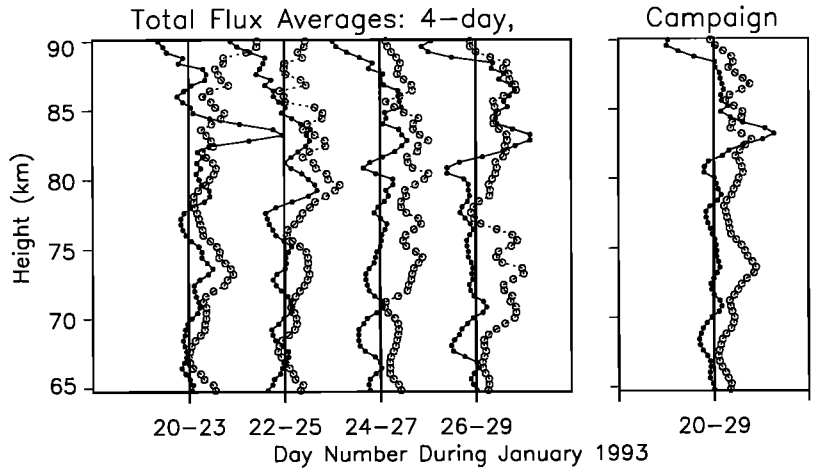

Figure 15. Overlapping 4-day and campaign estimates of zonal momentum flux (open dots) and meridional momentum flux (solid dots) in the mesosphere for the January 1993 campaign. Profiles are offset by $10\,m^2\,s^{-2}$.

wave, which was of unusually large amplitude during the January 1993 campaign [*Wu et al.*, 1993; *Deng et al.*, 1996; *D. C. Fritts et al.*, manuscript in preparation, 1997 *Palo et al.*, 1997] and weakly present during the August 1994 experiment [*Fritts et al.*, this issue].

Figure 16 shows spectra of momentum flux for the mesosphere. In this presentation the data are binned into 5 min averages and the velocities at adjacent heights are averaged together in a sliding three-height average to reduce data gaps. The dependence of the spectral peak amplitudes on frequency is somewhat different in the mesosphere as compared to the stratosphere (Figure 11). In the mesosphere, the largest amplitude spectral peaks were generally at periods of 10 min to 1 hour, while in the stratosphere the extreme low-end (<2 hours) and high-end (>20 min) spectral peaks were

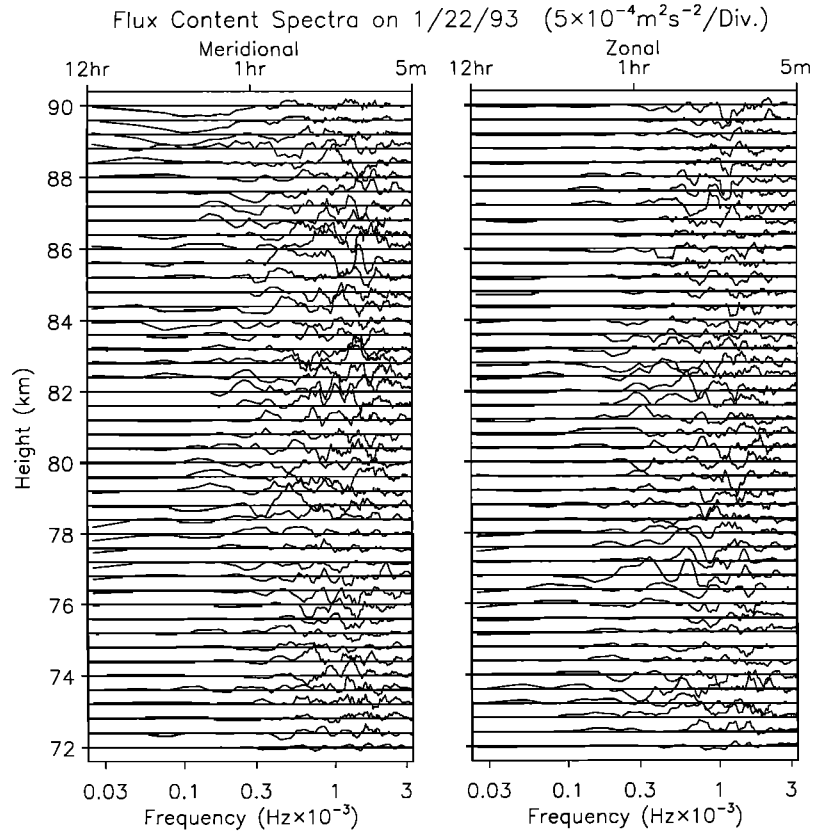

Figure 16. Same as Figure 11, but for the mesosphere. The spacing between horizontal grid lines is $5\times10^{-4}\,m^2\,s^{-2}$.

typically more important. When comparing spectra of momentum fluxes in the stratosphere and the mesosphere it should be remembered that the processing was not exactly the same in the two cases. In the mesosphere, the vertical averaging could have suppressed the contribution from waves with short vertical wavelengths. However, even at high frequencies the spectral peaks are fairly well correlated over height intervals greater than the distance (1.2 km) over which the data were vertically averaged, and those waves with short vertical wavelengths are unlikely to contribute much flux in any event.

Isotropically propagating wave packets is fairly apt as a description for the high-frequency gravity waves in the mesosphere, as well as the stratosphere. Because of data gaps, we were unable to perform the correlation analysis to look at the time evolution of the waves responsible for particular spectral peaks as we did in the stratosphere.

6. Summary and Conclusions

By performing least squares fits to the velocity time series we found dominant IGW periods of 1.5 days and 2.1 days for the January 1993 and August 1994 experiments, respectively. For the January 1993 experiment, a fit was obtained for the vertical velocity component as well as for the horizontal components. The amplitude of the vertical wave component was small ($<0.1\,\mathrm{m\,s^{-1}}$), but measurable with the Jicamarca radar and somewhat larger than would be predicted on the basis of the orbital ellipses in the horizontal plane. It follows then that the intrinsic period estimated using the vertical velocities was somewhat shorter than predicted from the orbital ellipses. The vertical velocities also yielded estimates of inertial period with much less scatter than the values inferred from the orbital ellipses. Our results suggest that vertical velocities can be used for IGW parameter estimation by powerful radars like Jicamarca and the new generation of lidars.

Caution should be exercised when comparing momentum fluxes between experiments as the estimates could be affected by different beam configurations, range resolutions, time resolution, time integration, or different algorithms. The estimates presented in this paper were formed by including only samples which were measured simultaneously on a coplanar beam pair. The momentum fluxes obtained in this manner were better as judged by the consistency of the estimates with height. We found that most of the momentum flux was carried by waves at periods $\geq$4 hours in the stratosphere and $\geq$1 hour in the mesosphere. Further work is clearly needed to establish the best estimators for momentum flux and the dominance of low frequencies in our results suggests that deterministic treatments (as opposed to purely statistical treatments) of momentum flux should be considered.

The weakness of the QBO [e.g., *Hayashi and Golder,* 1994] and the MSAO [*Hamilton et al.,* 1995] in eddy-resolving general circulation models (GCMs) of the middle atmosphere is generally attributed to a missing dynamical stress. The discrepancy between model predictions and observations is larger for the QBO, especially for the descent of westward shear zones [*Takahashi and Boville,* 1992; *Dunkerton,* this issue]. Reasonable agreement can only be achieved by adding momentum flux in the form of a parameterization. It has been argued that the unresolved sub-grid-scale waves are the source of the missing flux [*Hayashi and Golder,* 1994; *Hamilton,* 1995]. However, other GCM simulations [*Takahashi and Kumara,* 1995] and radiosonde balloon observations [*Maruyama,* 1994; *Sato and Dunkerton,* this issue] indicate a crucial role for IGW fluxes in maintaining the QBO. Although the experimental evidence remains quite fragmentary, our results may be taken as further evidence supporting the importance of IGW fluxes.

Thin layers of enhanced momentum flux were sometimes seen in the lower stratosphere. The obvious anticorrelation between the shear of the mean wind and the momentum flux in these layers suggests that they were associated with *in situ* generation of the Kelvin-Helmholtz instability rather than gravity waves propagating from lower levels. At short periods, momentum flux spectra in the stratosphere and mesosphere showed numerous positive and negative peaks, suggesting that the short-scale waves are fairly isotropic in their direction of propagation, and usually carry little net momentum due to cancellation. Over a few isolated intervals in time and height, the momentum flux associated with high frequencies increased markedly, but we lack the auxiliary data that would allow us to relate these events to changes in atmospheric conditions. At middle and high latitudes, shorter-wavelength waves may play a much greater role, although simple theoretical arguments made in section 5 did not indicate the change in the inertial cutoff period with latitude to be in itself a significant factor. Diffusivity was not considered in section 5, but it could preferentially act to cause more damping of long-wavelength waves at high latitudes [*Marks and Eckermann,* 1995].

Acknowledgments. This research was supported by the NSF under grants ATM-9118899 and ATM-9214657. We thank the Director, Ronald Woodman, and the staff of Jicamarca Radio Observatory (JRO) for their assistance in carrying out the experiment. JRO is operated by the Geophysical Institute of Perú, Ministry of Education. We are grateful to Kevin Hamilton for helpful comments. One of the authors (D. R.) thanks the Geophysical Fluid Dynamics Institute at Florida State University and the Radio Atmospheric Science Center at Kyoto University for facilitating the completion of this work.

References

Cadet, D., and H. Teitelbaum, Observational evidence of internal inertia-gravity waves in the tropical stratosphere, *J. Atmos. Sci., 35,* 892–907, 1979.

Cho, J. Y. N., Inertio-gravity wave parameter estimation from cross-spectral analysis, *J. Geophys. Res., 100,* 18,727–18,737, 1995.

Cornish, C. R., and M. F. Larsen, Observations of low-frequency inertia-gravity waves in the lower stratosphere over Arecibo, *J. Atmos. Sci., 46,* 2428–2439, 1990.

Deng, W., J. E. Salah, R. R. Clark, S. J. Franke, D. C. Fritts, P. Hoffmann, D. Kuerschner, A. H. Manson, C. E. Meek, D. Murphy, T. Nakamura, S. E. Palo, D. M. Riggin, R. G. Roble, R. Schminder, W. Singer, T. Tsuda, R. A. Vincent, and Q. Zhou, Coordinated global radar observations of tidal and planetary waves in the mesosphere and lower thermosphere during 20–30 January 1993, Submitted to *J. Geophys. Res.,* 1996.

Dunkerton, T. J., The role of gravity waves in the quasi-biennial oscillation, *J. Geophys. Res.,* this issue, 1997a.

Eckermann, S. D., Hodographic analysis of gravity waves: Relationships among Stokes parameters, rotary spectra and cross-spectral methods, *J. Geophys. Res., 101,* 19,169–19,174, 1996.

Eckermann, S. D., and W. K. Hocking, Effect of superposition on measurements of atmospheric gravity waves: A cautionary note and reinterpretations, *J. Geophys. Res., 94,* 6333–6339, 1989.

Eckermann, S. D., I. Hirota, and W. K. Hocking, Gravity wave and equatorial wave morphology of the stratosphere derived from long-term rocket soundings, *Q. J. R. Meteorol. Soc., 121,* 149–186, 1995.

Fritts, D. C., Gravity wave saturation in the middle atmosphere: A review of theory and observations, *Rev. Geophys., 22,* 275–308, 1984

Fritts, D. C., and P. K. Rastogi, Convective and dynamical instabilities due to gravity wave motions in the lower and middle atmosphere: Theory and observations, *Radio Sci., 20,* 1247–1277, 1985.

Fritts, D. C., and R. A. Vincent, Mesospheric momentum flux studies at Adelaide, Australia: Observations and a gravity wave/tidal interaction model, *J. Atmos. Sci., 44,* 605–619, 1987.

Fritts, D. C., T. Tsuda, T. E. VanZandt, S. A. Smith, T. Sata, S. Fukao, and S. Kato, Studies of velocity fluctuations in the lower atmosphere using the MU Radar. Part II: Momentum fluxes and energy densities, *J. Atmos. Sci., 47,* 51–66, 1990.

Fritts, D. C., L. Yuan, M. H. Hitchman, L. Coy, E. Kudeki, and R. F. Woodman, Dynamics of the equatorial mesosphere observed using the Jicamarca MST radar during June and August 1987, *J. Atmos. Sci., 49,* 2353–2371, 1992.

Fritts, D. C., J. F. Garten, D. M. Riggin, R. A. Goldberg, G. A. Lehmacher, F. J. Schmidlin, S. McCarthy, C. D. Fawcett, E. Kudeki, M. H. Hitchman, R. Lieberman, and R. A. Vincent, Equatorial dynamics observed by rocket, radar, and satellite during the CADRE/MALTED Campaign, *J. Geophys. Res.,* this issue, 1997b.

Fukao, S., T. Sato, T. Tsuda, S. Kato, M. Inaba, and I. Kimura, VHF Doppler radar determination of the momentum flux in the upper troposphere and lower stratosphere: Comparison between the 3- and four-beam methods, *J. Atmos. Oceanic Technol., 5,* 57–69, 1988.

Hamilton, K., Climatological statistics of stratospheric inertia-gravity waves deduced from historical rocketsonde wind and temperature data, *J. Geophys. Res., 96,* 20,831–20,839, 1991.

Hamilton, K., R. J. Wilson, J. D. Mahlman, and L. J. Umscheid, Climatology of the SKYHI troposphere-stratosphere-mesosphere general circulation model, *J. Atmos. Sci., 52,* 5–43, 1995

Hamilton, K., Comprehensive simulation of the middle atmospheric climate: some recent results, *Climate Dyn., 11,* 223–241, 1995.

Hayashi, Y., and D. G. Golder, Kelvin and mixed Rossby-gravity waves appearing in the GFDL "SKYHI" general circulation model and the FGGE dataset: Implication for their generation mechanism and role in the QBO, *J. Meteorol. Soc. Jpn., 72,* 901–935, 1994.

Hines, C. O., Generalization of the Richardson criterion for the onset of atmospheric turbulence, *Q. J. R. Meteorol. Soc., 97,* 429–439, 1971.

Hines, C. O., Tropopausal mountain waves over Arecibo: A case study, *J. Atmos. Sci., 46,* 476–488, 1989.

Hirota, I., Equatorial waves in the upper stratosphere and mesosphere in relation to the semiannual oscillation of the zonal wind, *J. Atmos. Sci.,* it 35, 714–722, 1978.

Hirota, I., and T. Niki, A statistical study of inertia-gravity waves in the middle atmosphere, *J. Meteorol. Soc. Jpn., 63,* 1055–1065, 1985.

Hitchman, M. H., K. W. Bywaters, D. C. Fritts, L. Coy, E. Kudeki, and F. Surucu, Mean winds and momentum fluxes over Jicamarca, Peru, during June and August 1987, *J. Atmos. Sci., 49,* 2372–2383, 1992.

Hitchman, M. H., J. M. Kugi, G. A. Postel, C.-Y. Yao, V. L. Harvey, E. Kudeki, C. Fawcett, D. C. Fritts, D. Riggin, and D. Ortland, Mean winds in the tropical stratosphere and mesosphere during January 1993, March 1994, and August 1994, *J. Geophys. Res.,* this issue, 1997.

Karoly, D. J., G. L. Roff, and M. J. Reeder, Gravity wave activity associated with tropical convection detected in TOGA COARE sounding data, *Geophys. Res. Lett., 23,* 261–264, 1996.

Lieberman, R. S., and P. B. Hays, An estimate of the momentum deposition in the lower thermosphere by the observed diurnal tide, *J. Atmos. Sci., 51,* 3094–3105, 1994.

Maekawa, Y., S. Fukao, T. Sato, S. Sato, and R. F. Woodman, Internal inertia-gravity waves in the tropical lower stratosphere observed by the Arecibo Radar, *J. Atmos. Sci., 41,* 2359–2367, 1984.

Maruyama, T., Upward transport of westerly momentum due to disturbances of the equatorial lower stratosphere in the period range of about 2 days.—A Singapore data analysis for 1983–1993, *J. Meteorol. Soc. Jpn., 72,* 423–431, 1994.

Marks, C. J., and S. D. Eckermann, A three-dimensional nonhydrostatic ray-tracing model for gravity waves: Formulation and preliminary results for the middle atmosphere, *J. Atmos. Sci.,* , *52,* 1959–1984, 1995.

McAfee, J. R., B. B. Balsley, and K. S. Gage, Momentum flux measurements over mountains: Problems associated with the symmetrical two-beam radar Technique, *J. Atmos. Oceanic Technol., 6,* 500–508, 1989.

Murphy, D. A., and R. A. Vincent, Estimates of momentum flux in the mesosphere and lower thermosphere over Adelaide, Australia, from March 1985 to February 1986, *J. Geophys. Res., 98,* 18,617–18,638, 1993.

Nakamura, T., T. Tsuda, M. Yamato, S. Fukao, and S. Kato, Characteristics of gravity waves in the mesosphere observed with the Middle and Upper Atmosphere Radar, 1. Momentum flux, *J. Geophys. Res., 98,* 8899–8910, 1993.

Nielsen, J. W., In situ observations of Kelvin-Helmholtz Waves along a frontal inversion, *J. Atmos. Sci., 49,* 369–386, 1992.

Palmer, T. N., G. N. Shutts, and R. Swindbank, Alleviation of a systematic bias in general circulation and numerical weather prediction models through an orographic gravity wave drag parameterization. *Q. J. R. Meteorol. Soc., 112,* 1001–1040, 1986.

Palo, S. E., and S. K. Avery, Observations of the quasi-two-day wave in the middle and lower atmosphere over Christmas Island, *J. Geophys. Res., 101,* 12,833–12,846, 1996.

Palo, S. E., et al., An intercomparison between the GSWM, UARS and ground based radar observations: A case study in January 1993, Ann. Geophys., in press, 1997.

Reid, I. M., and R. A. Vincent, Measurements of mesospheric gravity wave momentum fluxes and mean flow accelerations at Adelaide, Australia, *J. Atmos. Terr. Phys., 49,* 443–460, 1987.

Riggin, D., D. C. Fritts, C. D. Fawcett, and E. Kudeki, Observations of inertia-gravity wave motions in the stratosphere over Jicamarca, Peru, *Geophys. Res. Lett., 22,* 3239–3242, 1995.

Sato, K., F. Hasegawa, I. Hirota, Short-period disturbances in the equatorial lower stratosphere, *J. Meteorol. Soc. Jpn., 72,* 859–872, 1994.

Sato, K., T. J. Dunkerton, Estimates of momentum flux associated with equatorial Kelvin and gravity waves, *J. Geophys. Res.,* this issue, 1997.

Shimizu, A., T. Tsuda, Radiosonde observations of equatorial atmosphere dynamics over Indonesia, *J. Geophys. Res.,* this issue, 1997.

Spano, E., M. Crochet, and O. Ghebrebrhan, Some characteristics of the matrix used for the full decoding of truncated ranges, in *Solar-Terrestrial Energy Program: Proc. Fifth Workshop of Technical and Scientific Aspects of MST Radar,* B. Edwards (ed.), 439–445, 1991. Available from SCOTEP Secretariat, NOAA/NGDC, Boulder, CO.

Takahashi, M., and B. A Boville, A three-dimensional simulation of the quasi-biennial oscillation, *J. Atmos. Sci., 49,* 1020–1035, 1992.

Takahashi, M., and T. Kumakura, Equatorial wave behavior in a three-dimensional sector model: Relation to the simulated QBO-like oscillation and comparison with a T21 General Circulation Model, *J. Meteorol. Soc. Jpn., 73,* 1011–1027, 1995.

Trenberth, K. E., and J. G. Olson, An evaluation and intercomparison of global analyses from the National Meteorological Center and European Centre for Medium-Range Weather Forecasts, *Bull. Am. Meteorol. Soc., , 69,* 1047–1057, 1988.

Tsuda, T., Y. Murayama, H. Wiryosumarto, S. Woro, B. Harijono, and S. Kato, Radiosonde observations of equatorial atmosphere dynamics over Indonesia, 2. Characteristics of gravity waves, *J. Geophys. Res., 99,* 10,507–10,516, 1994.

Vincent, R. A., and I. M. Reid, HF Doppler measurements of mesospheric gravity wave momentum fluxes, *J. Atmos. Sci., 40,* 1321–1333, 1983.

Wu, D. L., P. B. Hays, W. R. Skinner, A. R. Marshall, M. D. Burrage, R. S. Lieberman, and D. A. Ortland, Observations of the quasi 2-day wave from the High Resolution Doppler Imager on UARS, *Geophys. Res. Lett., 20,* 2853–2856, 1993.

Yamanaka, M. D., S. Ogino, S. Kondo, T. Shimomai, S. Fukao, Y. Shibagaki, Y. Maekawa, and I. Takayabu, Inertio-gravity waves and subtropical multiple tropopauses: Vertical wavenumber spectra of wind and temperature observed by the MU radar, radiosondes and operational rawinsonde network, *J. Atmos. Terr. Phys.,* it 58, 785–805, 1996.

Young, H. D., *Statistical Treatment of Experimental Data,* 172 pp., McGraw-Hill, New York, 1962.

David C. Fritts and Dennis M. Riggin, Colorado Research Associates/NWRA, 3380 Mitchell Lane, Boulder, CO 80301. (e-mail: dave@michelangelo.colorado.edu; Dennis.Riggin@Colorado.edu)

Clinton D. Fawcett and Erhan Kudeki, Department of Electrical and Computer Engineering, CSRL MC-229, 1308 W. Main Street, University of Illinois, Urbana, IL 61801. (e-mail: cfawcett@uiuc.edu; erhan@deln.ece.uiuc.edu)

Matthew H. Hitchman, Department of Atmospheric and Oceanic Sciences, 1225 West Dayton Street, University of Wisconsin, Madison, WI 53706. (e-mail: matt@meteor.wisc.edu)

(Received April 18, 1996; revised November 19, 1996; accepted November 19, 1996.)